Organic Electronics 47 (2017) 228–234

Contents lists available at ScienceDirect

Organic Electronics

journal homepage: www.elsevier.com/locate/orgel

Review

Negative differential resistance in polymer tunnel diodes using atomic layer deposited, TiO_2 tunneling barriers at various deposition temperatures

Jeremy J. Guttman [a], Conner B. Chambers [a], Al Rey Villagracia [b], Prof. Gil Nonato C. Santos [b], Prof. Paul R. Berger [a, c, *]

[a] Department of Electrical and Computer Engineering, The Ohio State University, Columbus, OH 43210, United States
[b] Physics Department, De La Salle University, Manila, Metro Manila, Philippines
[c] Department of Physics, The Ohio State University, Columbus, OH 43210, USA

ARTICLE INFO

Article history:
Received 8 December 2016
Received in revised form
6 May 2017
Accepted 7 May 2017
Available online 10 May 2017

Keywords:
Quantum tunneling
Tunnel diodes
Conjugated polymers
Atomic layer deposition
Titanium dioxide
Oxygen vacancy defects
Density-of-States

ABSTRACT

Atomic layer deposition (ALD) presents a method to deposit uniform and conformal thin-film layers with a high degree of control and repeatability. Quantum functional devices that provide opportunities in low-power molecular and organic based memory and logic via thin metal-oxide tunneling layer were previously reported by Yoon et al. [1]. Demonstrated here area polymer tunnel diodes (PTD) with high negative differential resistance (NDR) using an ALD deposited tunneling layer grown between 250 °C – 350 °C. A critical relationship between deposition temperature, oxygen vacancy concentration and room temperature NDR is presented. In this work, for a TiO_2 deposition temperature of 250 °C, the peak NDR voltage position (V_{peak}) and associated peak current density (J_{peak}) are ~4.3 V and −0.14 A/cm^2, respectively, with a *PVCR* as high as 1.69 while operating at room temperature. The highest PVCR recorded was 4.89 ± 0.18 using an ALD deposition temperature of 350 °C. The key advantages of the ALD process used in fabrication of PTDs are increased repeatability and manufacturability.

Contents

1. Introduction

In recent years, there have been tremendous advances in all facets of electronics technology. Specifically, organic electronic devices, such as OLEDs [2–5] and OFETs/OTFTs [6–8], have come a long way in regards to efficiency and performance. Recently, organic based technologies have gained a significant amount of attention and growth, with expectations to reach approximately $70B in market revenue by 2026 [9]. In particular, plastic volatile memory and RF logic devices would present a viable alternative for low-cost manufacturing. And so, the opportunity will exist for flexible, low cost, low-power organic based memory and logic

* Corresponding author. Department of Electrical and Computer Engineering, The Ohio State University, Columbus, OH 43210, United States.
E-mail addresses: guttman.21@osu.edu (J.J. Guttman), chambers.267@osu.edu (C.B. Chambers), al.villagracia@dlsu.edu.ph (A.R. Villagracia), gil.santos@dlsu.edu.ph (G.N.C. Santos), pberger@ieee.org (P.R. Berger).

http://dx.doi.org/10.1016/j.orgel.2017.05.015
1566-1199/

circuitry.

Reports of NDR observed using metal-oxide junction devices were reported early on [10]. Hickmott observed rapid decreases in currents, suggesting trap centers within the oxide only accessible to energic electrons resulting in a negative resistance. Hickmott adds that the insulator thickness should not exceed 100 nm, nor be less than a minimum of 8 nm. The diodes presented here are nominally 6 nm. Pagnia and Sotnik further explain that one pathway to the NDR branch "originates from rupturing filaments …" and the other could be due to oxygen vacancies modulating conductivity, as later purported for memristor operation [11]. Emerging sometime later, hybrid organic/inorganic resistive switching devices were found to exhibit NDR while using a thin metal-oxide layer [12,13]. Though, historically the scope of experimentation as well as conceptual understanding have not been agreed upon. Bory et al. demonstrated organic resistive switching diodes using an anodic oxidized Al_2O_3 interfacial films. Interestingly, after "treating" the devices with an electroforming process, NDR was observed in the I-V characteristics. The NDR was thought to be the result of the breakdown of a double layer at the Al_2O_3/polymer induced by positive defects sites in the oxide resulting in "injection redistribution" [12]. Thermal imaging was also performed by Bory et al. to affirm the filamentary conduction. Thermal imaging has not been performed yet on the diodes presented here. This article offers alternative hypotheses on the NDR phenomena for hybrid organic/inorganic diodes all the while demonstrating optimized fabrication of highly reproducible NDR diodes without the use of *ex situ* defect density modifications or any electroforming process.

NDR seen in organic-based devices have also been studied previously and were first conceptualized using small molecules as the active semiconducting material [14]. Since then, NDR devices have intrigued researchers for their potential in low-power electronics [14–20], but the reported demonstrations have had limited yield, repeatability, and typically a non-optimal current-voltage shape for proper circuit latching behavior. In 2005, Yoon et al. [1] presented a polymer tunnel diode (PTD) that exhibited room temperature negative differential resistance (NDR) while exploring low-power memory [21] and logic [22] alternatives. The challenge was in generating low-power performance and successful demonstration of repeatable NDR with reasonably high peak-to-valley current ratios (*PVCR*) ($\sim \geq 2$) [23], a figure-of-merit in NDR tunnel diodes.

In general, for memory applications, peak current densities should be kept minimal while reducing valley currents for low-power consumption. Peak (J_{peak}) and valley currents densities (J_{valley}) are taken from the maximum and minimum tunneling currents, or peak and valley of NDR, respectively. A narrow current-voltage valley region in combination with the high *PVCR* and low NDR voltages at peak current, V_{peak}, allows for sharp turn-on voltages, low voltage latches, and therefore low-power digital circuitry. Minimal J_{valley} is necessary to reduce static power consumption for memory applications [24,25]. Alternatively, reducing J_{peak} of NDR will also reduce dynamic power dissipation.

In this work, Yoon et al.'s [1] findings are extended by demonstrating NDR behavior at room temperature in PTDs using a thin TiO_2 tunneling layer deposited via atomic layer deposition (ALD). In Yoon's previous report, the TiO_2 tunneling layer was synthesized by plasma oxidation of pure Ti metal atop indium tin oxide (ITO). It was found that in the absence of a thin metal-oxide layer, where either PEDOT:PSS was in direct contact with the electroactive polymer or the electroactive polymer was in direct contact with the ITO, NDR was not observed, but when a thin layer of TiO_2 was inserted, consistent and repeatable NDR was demonstrated under reverse-bias [1]. Here, a more in-depth explanation of the physical mechanisms behind the quantum tunneling for PTDs is considered. This is the first report since the seminal discovery of PTDs which uses ALD to synthesize a tunneling barrier.

2. Experimental section

The tunneling device resembles the basic structure of an OLED with the exception of a thin metal-oxide tunneling barrier placed between the polymer and anode. Indium-tin-oxide (ITO) deposited atop polished float glass [Delta-Technologies, ~60 nm thick, ~15 Ω/sq sheet resistance (R_s)] was used as both a substrate and the anode contact. ITO substrates were cleaned using solvents and patterned to define individual devices. The tunneling oxide was then conformably deposited atop the ITO via ALD. The thickness of the tunneling barrier was optimized based on the previous work [1], and therefore a target of 60–65 Å was used for TiO_2; the TiO_2 film was purposefully made thicker to eliminate the possibility of direct carrier tunneling or filamenting. Ellipsometry was performed post-ALD on a Si/SiO_2 monitor wafer to confirm the thickness of the ultra-thin TiO_2 films using a spectroscopic Woollam α-SE ellipsometer. Concerns on the average surface roughness (R_a) of ITO—R_a/RMS of 1.39/1.75 nm measured using atomic force microscopy (AFM)—resulted in the use of SiO_2 monitor wafers (R_a/RMS of 0.316/0.449 nm measured using AFM) included in each run for improved precision during ellipsometry measurements. Assuming that SiO_2 and ITO share similar wetting properties, a nominal thickness can be assumed for TiO_2 deposited on ITO.

A Picosun SUNALE R-150B ALD reactor fitted with a titanium tetrachloride ($TiCl_4$) precursor and H_2O oxidizer was used for the TiO_2 deposition. Parameters were set based on a series of optimization experiments to determine the precursor purge/pulse times for five different temperature regimes. A stable growth rate between runs (±0.02 Å/cycle) and temperatures (±0.03 Å/cycle) confirmed these experiments were done within the $TiCl_4$ ALD growth window. Deposition temperatures varied between 250 and 350 °C at 25 °C intervals to observe the dependence of tunneling and ALD deposition temperature. The temperature of deposition will further reveal a correlation between NDR performance and oxygen vacancy defect densities. *Ex situ* analytical measurements on the TiO_2 film were then employed using ultraviolet–visible spectroscopy (UV–Vis) and X-Ray Photoelectron Spectroscopy (XPS). XPS was used to verify conformal coverage of TiO_2 on ITO as well as to determine the relative concentration of oxygen vacancies based on the changes in Ti cation states. It should be mentioned that low relative concentrations of In or Sn were detected in the spectra, though this is more than likely the result of the escape depth of In and Sn XPS signals being greater than the TiO_2 film thickness.

After the completion of ALD, the samples were transferred directly into an inert atmosphere MBraun glovebox to avoid adsorption of water vapor, CO_2, and other contaminants from the air and for the final stages of fabrication. A thin film of a polymer semiconductor (Livilux PDY-132, Merck KGaA, "Super Yellow") was spin-coated atop the TiO_2 layer from a concentration of 0.4 % wt in a solution of 80% toluene and 20% tetrahydrofuran (THF). Spin-coated films were nominally ~35 nm thick measured using profilometry. After transfer to a second MBraun glovebox through a shuttle loadlock to further avoid air exposure, an Al cathode was evaporated through a shadow mask at a rate of ~2–3 Å/s at a vacuum level $<3 \times 10^{-6}$ Torr to complete fabrication. Evaporated Al films were nominally 250 nm thick. The final devices each formed an active area of 0.28 cm^2. Electrical characterization measurements were taken using a Cascade REL-4830HT probe station with triaxial shielding and data collected via a Keysight B1500A parametric analyzer in ambient air, under dark conditions at room temperature.

The density-of-states of different systems of PDY-132 were also investigated using density functional theory (DFT) [26–34]. The structure of PDY-132 is shown in Fig. 1. The periodicity of the structure is oriented along the z-axis while vacuum space is placed along x- and y-axis to avoid interactions with its adjacent systems. All geometric structures were optimized. The Perdew-Burke-Ernzerhof (PBE) generalized gradient approximation was implemented with an exchange-correlation function [30,32]. Monkhorst-Pack scheme of 1 × 1 × 15 was employed for special points following sample integration over the Brillouin zone [31]. Geometry optimization of (1:N:N) PDY-132 with different ratio of components (N = 1–3) for its unit cell were carried out using spin unrestricted; all electron DFT calculations with double numerical and d-functions basis set with the Tkatchenko-Scheffler van der Waals correction [28,31]. The convergence threshold for maximum energy change, maximum force and maximum displacement are 10^{-6} Ha, 0.002 Ha/Å, and 0.005 Å, respectively [28]. A global orbital cutoff of 3.700 Å was employed. Finally, multi-core parallel computing was carried out using the parallel eigenvalue solution of Auckenthaler *et al* [28].

3. Results and discussion

In Fig. 2, typical representative PTD's are presented for each ALD deposition temperature, confirming highly reproducible and consistent NDR in the quadrant III reverse-bias range (sweeping the voltage from 5 to −10 V). For a TiO_2 deposition with a substrate temperature of 250 °C, J_{peak} and J_{valley} were −0.14 A/cm^2 and -0.08 A/cm^2, respectively, with a *PVCR* of 1.69. This was repeatable over 6–8 consecutive sweeps with an average variation of ±0.015 A/cm^2 for J_{peak} and ±0.17 V for V_{peak}. Additionally, yield was excellent with every PTD across the samples exhibiting reportable NDR. It was observed that in general, the *PVCR* increases with the deposition temperature with the average lowest reported *PVCR* of 1.56 occurring for TiO_2 grown at 275 °C and the highest *PVCR* of 4.89 for TiO_2 grown at 350 °C.

Reverse bias *I-V* characteristics of diodes without the TiO_2 tunneling barrier (ITO/PDY-132/Al) were used as a control [Fig. 2 (f)]. The data shows that without the TiO_2 tunneling oxide, some intermittent characteristic feature appears between −3 and −4 V [Fig. 2 (f)]. However, this feature was not consistent, or repeatable, and falls in the category of anomalous current found in countless other reports on OLEDs with ITO used as the anode [35–37].

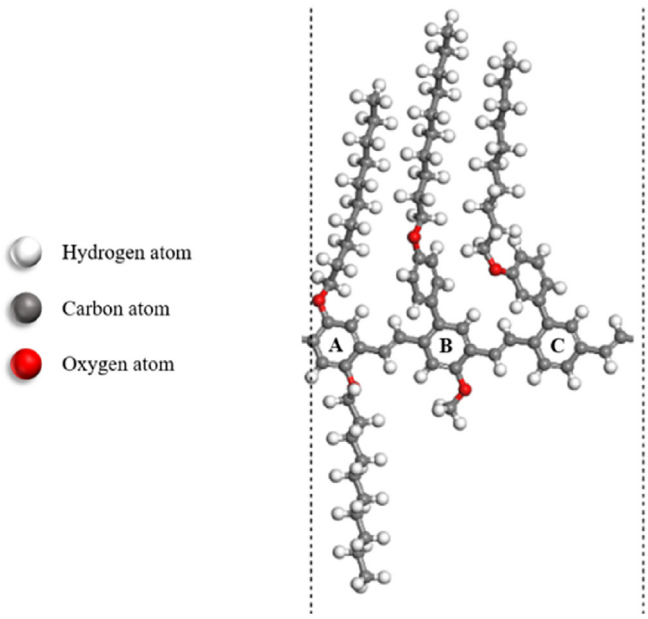

Fig. 1. The chemical structure of PDY-132, "Super Yellow" in ball and stick figure $[A]_1[B]_N[C]_N$.

Table 1 summarizes the *I-V* characteristics of multiple devices including the J_{peak}, J_{valley}, V_{peak}, and V_{valley} for each deposition temperature along with the associated *PVCR*. It is observed that by varying TiO_2 deposition temperature of ALD, there appears an accompanying change in J_{peak}. A temperature range between 250 and 350 °C is chosen based on previous reports of ALD using $TiCl_4$ and H_2O as precursors [38,39]. Interestingly, TiO_2 undergoes a phase change between 200 °C and 300 °C, resulting in an obvious change in the microstructure of the crystals [40]. According to literature [39–41], the films deposited near 300 °C are more than likely mixed phase between anatase and rutile while the rutile phase exists in TiO_2 films for ALD temperatures above 350 °C [40]. A deposition temperature of 250 °C was used as the starting point in this investigation of deposition temperature on PTD performance. It is theorized that as the temperature of deposition increases, there exists a change in oxygen vacancy concentration [42] that can be monitored in XPS spectra as a shift of the Ti 4^+ cation state to lower Ti oxidation states in the form of sub-oxide compositions, TiO_{x-2}. Due to the minimum cracking temperatures of the $TiCl_4$ precursor to release the Ti atom, depositions below 250 °C were not explored here.

XPS spectra were gathered for TiO_2 grown at 250–350 °C at 25 °C increments using a Kratos Axis Ultra XPS system. Estimation of the various identifiable states of Ti are quantified after subtracting a Shirley-type background [43] from the spectral components and fitting with Gaussian/Lorentzian line shapes. Due to the low relative concentrations present, Ti 2^+ and 3^+ are difficult to decipher from one another and therefore are grouped together during quantification. A slight increase in the 2^+ and 3^+ is observed as the temperature of deposition increases. Correlating the XPS data to the *I-V* plots of Fig. 2 along with the assumption that sub-oxide concentrations can be linked to oxygen vacancy defects in the film, an increase in the vacancy concentration at higher temperatures has a subsequent effect of increasing NDR tunneling currents.

Evidence presented by Li et al. shows the TiO_2 phase leads to effects on the formation energies of subsurface and surface oxygen vacancies resulting in varying concentrations [44]. An initial belief is that for an increase in oxygen vacancy concentration there would be an accompanying increase in J_{peak} and therefore *PVCR*. Assuming a well-defined energy trap level, it would allow for first order correlation between the defect density and *PVCR* dependent on the TiO_2 polymorph. Yet, when the *PVCR* versus temperature is observed in Table 1, it appears this is not necessarily the case, demonstrating that the task of purposefully introducing oxygen vacancies in the hope of improving PTD performance is not so trivial. Proportionality between J_{valley} and *PVCR* for instance at 325 °C (Table 1), makes it likely that there are other mechanisms at play. Leakage pathways from "excess current," or current that is not due to tunneling or diffusion [45], may in fact be increasing with deposition temperature due to interactions and surface defects at the interface between the ITO and TiO_2 caused by the elevated temperature or impurities in the TiO_2 producing surface trap states. Mixed-phased films could be causing local variations in the energy-band distribution of TiO_2 resulting in multi-energy level trapping. Furthermore, any device-to-device variation is more than likely attributed to the surface roughness of ITO. Nevertheless, a correlation appears to exist by which TiO_2 grown at higher temperatures shows improved *PVCR*. As the phase changes to more rutile, it may be that there is a shift in where oxygen vacancy energies reside within the energy-band distribution, becoming more distinct in

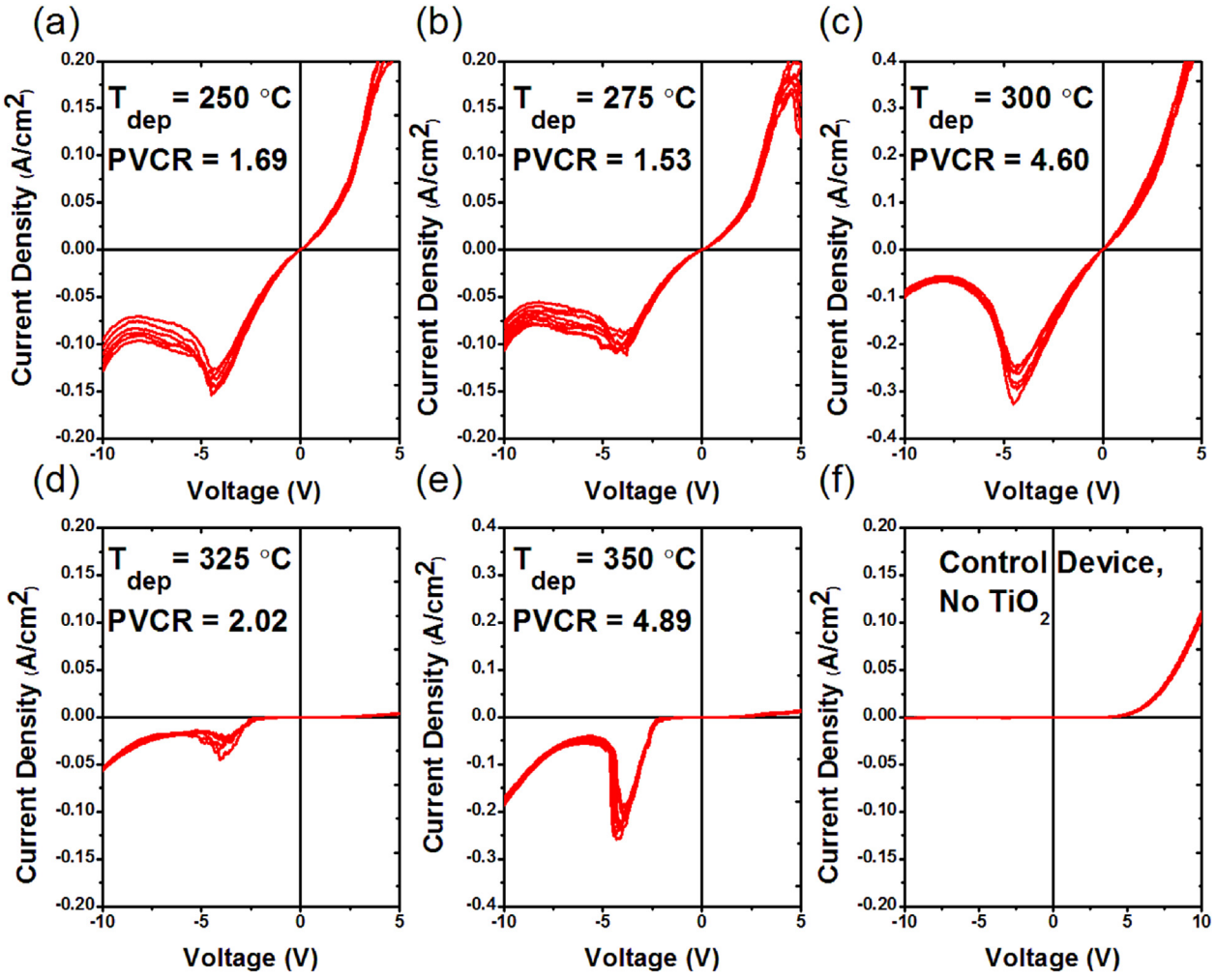

Fig. 2. *I-V* characteristics from 5 to −10 V of the polymer tunnel diodes exhibiting NDR in the reverse bias regime. Illustrated are PTDs with TiO_2 grown at (a) 250 °C, (b) 275 °C, (c) 300 °C, (d) 325 °C, (e) 350 °C, and (f) bare ITO used as control. Included are averaged *PVCR* ratios at the voltage of peak current.

Table 1
Calculated values of NDR peak current density (J_{peak}), voltage at peak current density (V_{peak}), NDR valley current density (J_{valley}), voltage at the valley current density (V_{valley}) and *PVCR* based on the *I-V* curves in Fig. 2 for TiO_2 tunneling barriers grown at 250, 275, 300, 325 and 350 °C. Result reflect devices with consistent performance.

Substrate temp (°C)	J_{peak} (A/cm^2)	V_{peak} (V)	J_{valley} (A/cm^2)	V_{valley} (V)	*PVCR*
250	−0.14 ± 0.009	−4.37 ± 0.15	−0.08 ± 0.009	−8.12 ± 0.11	1.69 ± 0.13
275	−0.10 ± 0.008	−4.12 ± 0.25	−0.07 ± 0.008	−8.40 ± 0.10	1.53 ± 0.17
300	−0.28 ± 0.029	−4.40 ± 0.06	−0.06 ± 0.004	−8.03 ± 0.12	4.60 ± 0.24
325	−0.03 ± 0.008	−3.96 ± 0.21	−0.02 ± 0.001	−5.55 ± 0.50	2.02 ± 0.35
350	−0.23 ± 0.023	−4.13 ± 0.18	−0.05 ± 0.005	−5.74 ± 0.17	4.89 ± 0.18

energy and accessible for electronic transport. This can be observed in Table 1's V_{valley} that shifts from nominally −8 V from 250 to 300 °C to −5.5 V at 325 °C. Perhaps by aiming for a single phase, more oxygen deficient film, for instance by growing purely amorphous TiO_2 [46–48], a subsequent increase in J_{peak} will be seen and higher, sharper *PVCR* will be observed. As such, *PVCR* may be controllable through modification of TiO_2 properties.

UV–Vis measures the optical bandgap of TiO_2 and yielded a value of 3.39 ± 0.06 eV for a deposition performed at a temperature of 250 °C and 3.27 ± 0.05 eV at 350 °C. Interestingly, other reports have shown that the bandgap of TiO_2 decreases for films that are more rutile [49]. This was observed in the UV–Vis data presented here, where a 0.12 ± 0.08 eV decrease in bandgap was observed from films deposited at 250 °C to ones deposited at 350 °C. The apparent optical shift may be due to the energy-band properties of the TiO_2 polymorph but an alternative theory is that a more pronounced defect state below the conduction band could lead to a shift in the onset of photoexcitation. Such would confirm again that the oxygen vacancy concentration increases with the temperature of ALD.

The tunneling mechanism for these PTDs is non-standard as increasing the tunneling barrier thickness does not show an exponential decay in peak current density. Moreover, samples were fabricated to have a thicker TiO_2 barrier in order to eliminate the possibility of direct tunneling [1]. Therefore, the tunneling occurring is most likely facilitated by intrinsic oxygen vacancies that produce a defect band in the TiO_2 barrier below the conduction band minima (CBM). Moreover, given the conformal and uniform

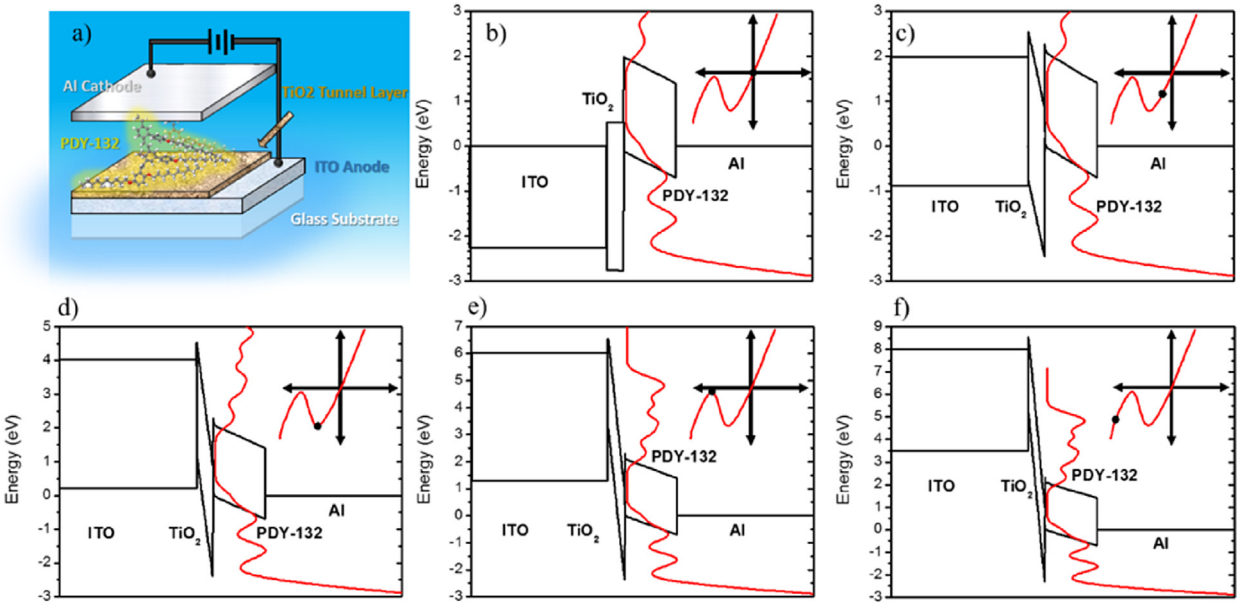

Fig. 3. 1-dimensional energy-band diagram of a polymer tunnel diode under various biasing conditions. Energy-band diagrams were generated using Silvaco software. (a) The structure of PTD using PDY-132 as the active polymer; (b) equilibrium band diagram; reverse bias of (c) −2 V; (d) −4 V; (e) −6 V; (f) −8 V.

nature of ALD deposited TiO_2 films, leakage currents greater than the NDR phenomena are not viable. Direct tunneling, described by quantum mechanics, maintains that in doubling the thickness of a potential barrier, an exponential reduction of free carriers able to penetrate the barrier would follow [25]. From previous reports, the reader is advised that these PTD devices do not follow this trend [1]. The NDR observed for these PTDs is most likely the result of two sequential “double-barrier” tunneling events. Therefore, the onset of conduction is thought to occur as a result of a trap-based tunneling event caused by tunneling from local defect sites or capture and emission from defect states located inside the TiO_2 barrier. Under an applied bias, the tunneling current exhibited is most likely dominated by a combination of “hopping” conduction—electrons tunneling between trap sites—and Frenkel-Poole Emission (FPE) conduction [50,51]. As mentioned previously, these traps are the result of oxygen vacancies and form a defect level below the CBM [44,52]. Under moderately applied fields, NDR is observed as a product of the detuning of the density-of-states (DOS) in lowest unoccupied molecular orbital (LUMO) of the polymer with the conduction band of the ITO connected through the trap level in the oxide. Under extremely high reverse-bias fields, the current is the result of thermionic emission over the barrier, or some breakdown mode of operation.

This device topology bears some similarity to reports of memristors [53], however, the operation of these PTDs is distinctly differentiated. First of all, a memristor uses a cube of TiO_2, which is sometimes up to 40 nm thick and the oxygen vacancies, which act as n-type dopants within the TiO_2, drift through this cube when an external bias is applied, shifting the TiO_2's resistivity. Essentially, as the name suggests, a resistor with memory of its previous bias. Whereas, the PTDs reported here are only ~6 nm thick and are already saturated with oxygen vacancies, as driven by the nontraditional, optimized ALD deposition conditions used here. Further, the I-V data shown in Strukov et al.'s first memristor report [54], as well as their 2004 report incorporating Langmuir Blodgett organic molecules, all show almost linear resistor I-V curves intersecting the origin, and this linear slope of resistance simply switches between high and low resistances, often with pronounced symmetry [55]. However, the PTDs exhibit a distinct NDR region where the current decreases with increasing voltage bias. Further, after the TiO_2 deposition shifts to a more rutile state at the higher deposition temperatures, the NDR behavior is superimposed upon a rectifying diode, which shows a low current in forward bias, and a rising current in reverse bias. Indeed, this N-shaped characteristic is exactly what facilitates the formation of tunnel diode memories and latches.

A brief description of the proposed NDR phenomena for PTDs as it relates to the density-of-states for PDY-132 is provided in Fig. 3. Available states in the LUMO of PDY-132, supplied by carriers in the ITO, satisfy the pre-condition for tunneling. A density functional theory (DFT) analysis was performed on PDY-132 to generate a DOS profile. Under no applied bias [Fig. 3 (b)], the system is at equilibrium. As a reverse-bias is applied [Fig. 3 (c)], free electrons from the ITO begin to tunnel into the available states in the LUMO band of the polymer. At some bias, there reaches a maximum carrier tunneling probability [Fig. 3 (d)], where the peak conduction band distribution aligns with the trap level of the TiO_2 tunneling barrier. Past this point [Fig. 3 (e)], the defect level of TiO_2 and conduction band of the polymer detune, resulting in the characteristic NDR. Under high reverse-bias [Fig. 3 (f)], the device reaches most likely direct tunneling, with electrons being directly supplied to the LUMO of PDY-132.

The primary objective of this report was to both fabricate and characterize PTDs using ALD to deposit TiO_2 ultra-thin tunneling barriers for the first time. Fabrication temperature is of particular interest for organic-based devices as lower temperature ALD would be favorable in the realization of functional circuity atop flexible plastic substrates. Additionally, from a cost perspective, fabrication should be completed in a minimal amount of steps to reduce the cost of processing. High production costs would defeat the purpose of using the low cost organic materials. Exploring deposition alternatives such as ALD to deposit pristine films all the while using their intrinsic properties would lend to be a decisive advantage in the device fabrication. By using only the process knobs offered by ALD to create the desired film properties, device manufacturing becomes more repeatable and robust as opposed to two-step oxide formations used previously [1,56].

4. Conclusion

It has been reported that the ALD temperature during the deposition of TiO_2 ultra-thin films can have a profound impact on the electrical properties of PTDs. In particular, the change of the TiO_2 phase from anatase to rutile was accompanied by a general increase in the *PVCR* occurring at higher deposition temperatures. It was suggested that the NDR behavior observed in PTD is a result of tunneling through localized defect sites in the TiO_2 layer. In comparing the density of state of PDY-132 with this defect level, a clear and accessible energy level exists which carriers can tunnel through. As the density of oxygen vacancies increases, the consequence of increasing the ALD deposition temperature, improved performance was observed.

Acknowledgements

The authors would like to acknowledge funding from the National Science Foundation (ECCS-1002240 and ECCS-1609299). The authors would like to thank Prof. Don Lupo for technical discussions that lead to the more processible substitution of PDY-132 as the active organic semiconductor, which should permit printing tests together, and Picosun for their continued interest and support.

References

[1] W.-J. Yoon, S.-Y. Chung, P.R. Berger, S.M. Asar, Room-temperature negative differential resistance in polymer tunnel diodes using a thin oxide layer and demonstration of threshold logic, Appl. Phys. Lett. 87 (2005) 203506.
[2] S. Byford, Samsung's Galaxy Round is the First Phone with a Curved Display, The Verge, 2013.
[3] N. Hagen, DuPont Displays and Kateeva Collaborate to Optimize Inkjet Printing for Mass Production of OLED TVs, Dupont Press Release, 2015.
[4] M. Kanellos, Start-up Creates Flexible Sheets of Light, CNET, 2007.
[5] A. Lemke, New OLED Luxury Luminaire Series Launched Under German Brand Name Liternity®, Liternity Press Release, 2011.
[6] C. Dimitrakopoulos, S. Purushothaman, J. Kymissis, A. Callegari, J. Shaw, Low-voltage organic transistors on plastic comprising high-dielectric constant gate insulators, Science 283 (1999) 822–824.
[7] P. Harrop, Plastic Logic Offer In-depth Look at Plastic Electronics Technology, IDtechEx, 2012.
[8] M. Noda, N. Kobayashi, M. Katsuhara, A. Yumoto, S. Ushikura, R. Yasuda, N. Hirai, G. Yukawa, I. Yagi, K. Nomoto, 47.3: a Rollable AM-OLED Display Driven by OTFTs, Wiley Online Library, 2010, pp. 710–713.
[9] D. Raghu, H. Peter, Printed, Organic & Flexible Electronics Forecasts, Players & Opportunities 2016-2026, 2016.
[10] T.W. Hickmott, Low-frequency negative resistance in thin anodic oxide films, J. Appl. Phys. 33 (1962) 2669–2682.
[11] H. Pagnia, N. Sotnik, Bistable switching in electroformed metal–insulator–metal devices, Phys. Status Solidi A 108 (1988) 11–65.
[12] B.F. Bory, P.R. Rocha, H.L. Gomes, D.M. De Leeuw, S.C. Meskers, Unipolar resistive switching in metal oxide/organic semiconductor non-volatile memories as a critical phenomenon, J. Appl. Phys. 118 (2015) 205503.
[13] R. Muller, C. Krebs, L. Goux, D.J. Wouters, J. Genoe, P. Heremans, S. Spiga, M. Fanciulli, Bipolar resistive electrical switching of CuTCNQ memories incorporating a dedicated switching layer, IEEE Electron Device Lett. 30 (2009) 620–622.
[14] I.-W. Lyo, P. Avouris, Negative differential resistance on the atomic scale: implications for atomic scale devices, Science 245 (1989) 1369.
[15] P. Bedrossian, D.M. Chen, K. Mortensen, J.A. Golovchenko, Demonstration of the tunnel-diode effect on an atomic scale, Nature 342 (1989) 258–260.
[16] F.-R.F. Fan, J. Yang, L. Cai, D.W. Price, S.M. Dirk, D.V. Kosynkin, Y. Yao, A.M. Rawlett, J.M. Tour, A.J. Bard, Charge transport through self-assembled monolayers of compounds of interest in molecular electronics, J. Am. Chem. Soc. 124 (2002) 5550–5560.
[17] F.-R.F. Fan, R.Y. Lai, J. Cornil, Y. Karzazi, J.-L. Brédas, L. Cai, L. Cheng, Y. Yao, D.W. Price, S.M. Dirk, et al., Electrons are transported through phenylene-ethynylene oligomer monolayers via localized molecular orbitals, J. Am. Chem. Soc. 126 (2004) 2568–2573.
[18] N.P. Guisinger, M.E. Greene, R. Basu, A.S. Baluch, M.C. Hersam, Room temperature negative differential resistance through individual organic molecules on silicon surfaces, Nano Lett. 4 (2004) 55–59.
[19] A.V. Tivanski, G.C. Walker, Ferrocenylundecanethiol self-assembled monolayer charging correlates with negative differential resistance measured by conducting probe atomic force microscopy, J. Am. Chem. Soc. 127 (2005) 7647–7653.
[20] R.A. Wassel, G.M. Credo, R.R. Fuierer, D.L. Feldheim, C.B. Gorman, Attenuating negative differential resistance in an electroactive self-assembled monolayer-based junction, J. Am. Chem. Soc. 126 (2004) 295–300.
[21] J.P.A. Van Der Wagt, Tunneling-based SRAM, Proc. IEEE 87 (1999) 571–595.
[22] K. Maezawa, T. Akeyoshi, T. Mizutani, Functions and applications of monostable-bistable transition logic elements (MOBILE'S) having multiple-input terminals, IEEE Trans. Electron Devices 41 (1994) 148–154.
[23] R. Anisha, S.-Y. Park, P.R. Berger, 90 nm 32× 32 bit tunneling SRAM memory array with 0.5 ns write access time, 1 ns read access time and 0.5 Volt operation, IEEE Trans. Circuits Syst. I 58 (2011) 2432–2445.
[24] J.C. Ellenbogen, J.C. Love, Architectures for molecular electronic computers. I. Logic structures and an adder designed from molecular electronic diodes, Proc. IEEE 88 (2000) 386–426.
[25] N. Jin, S.Y. Chung, R. Yu, R.M. Heyns, P.R. Berger, P.E. Thompson, The effect of spacer thicknesses on Si-based resonant interband tunneling diode performance and their application to low-power tunneling diode SRAM circuits, IEEE Trans. Electron Devices 53 (2006) 2243–2249.
[26] P.M. Abanador, A. Villagracia, N. Arboleda Jr., M. David, First principle investigation of atomic hydrogen adsorption on Pd-doped MgB2, Philipp. Sci. Lett. 6 (2013) 176–181.
[27] T. Auckenthaler, V. Blum, H.J. Bungartz, T. Huckle, R. Johanni, L. Krämer, B. Lang, H. Lederer, P.R. Willems, Parallel solution of partial symmetric eigenvalue problems from electronic structure calculations, Parallel Comput. 37 (2011) 783–794.
[28] J. Baker, A. Kessi, B. Delley, The generation and use of delocalized internal coordinates in geometry optimization, J. Chem. Phys. 105 (1996) 192–212.
[29] N. Lee, J. Lee, T. Ryu, Y. Kim, Y. Lansac, Y.H. Jang, Doping graphene with ferroelectric β-PVDF polymer film: density functional theory calculation and molecular dynamics simulation, Sci. Adv. Mater 6 (2014) 2422–2427.
[30] T.M. McCormick, C.R. Bridges, E.I. Carrera, P.M. DiCarmine, G.L. Gibson, J. Hollinger, L.M. Kozycz, D.S. Seferos, Conjugated polymers: evaluating DFT methods for more accurate orbital energy modeling, Macromolecules 46 (2013) 3879–3886.
[31] H.J. Monkhorst, J.D. Pack, Special points for Brillouin-zone integrations, Phys. Rev. B 13 (1976) 5188.
[32] I.H. Nayyar, E.R. Batista, S. Tretiak, A. Saxena, D.L. Smith, R.L. Martin, Localization of electronic excitations in conjugated polymers studied by DFT, J. Phys. Chem. Lett. 2 (2011) 566–571.
[33] M.V.J. Rocha, H.W.P. Carvalho, V.H.V. Sarmento, A.F. Craievich, T.C. Ramalho, Structural characterization, thermal properties, and density functional theory studies of PMMA-maghemite hybrid material, Polym. Compos 37 (2016) 51–60.
[34] V.G. Ruiz, W. Liu, A. Tkatchenko, Density-functional theory with screened van der Waals interactions applied to atomic and molecular adsorbates on close-packed and non-close-packed surfaces, Phys. Rev. B 93 (2016) 035118.
[35] S. Berleb, W. Brütting, M. Schwoerer, Anomalous current-voltage characteristics in organic light-emitting devices, Synth. Met. 102 (1999) 1034–1037.
[36] G. Yu, Y. Liu, S. Zhou, F. Bai, P. Zeng, M. Zheng, X. Wu, D. Zhu, Anomalous current-voltage characteristics of polymer light-emitting diodes, Phys. Rev. B 65 (2002) 115211.
[37] V. Cimrová, D. Neher, Anomalous electrical characteristics, memory phenomena and microcavity effects in polymeric light-emitting diodes, Synth. Met. 76 (1996) 125–128.
[38] J. Aarik, A. Aidla, H. Mändar, V. Sammelselg, Anomalous effect of temperature on atomic layer deposition of titanium dioxide, J. Cryst. Growth 220 (2000) 531–537.
[39] R.L. Puurunen, J. Saarilahti, H. Kattelus, Implementing ALD layers in MEMS processing, ECS Trans. 11 (2007) 3–14.
[40] J. Aarik, A. Aidla, T. Uustare, V. Sammelselg, Morphology and structure of TiO 2 thin films grown by atomic layer deposition, J. Cryst. Growth 148 (1995) 268–275.
[41] J. Aarik, Atomic-layer growth of TiO2-II thin films, Philos. Mag. Lett. 73 (1996) 115–119.
[42] M.T. Greiner, L. Chai, M.G. Helander, W. Tang, Z. Lu, Transition metal oxide work functions: the influence of cation oxidation state and oxygen vacancies, Adv. Funct. Mater 22 (2012) 4557–4568.
[43] D.A. Shirley, High-resolution X-ray photoemission spectrum of the valence bands of gold, Phys. Rev. B 5 (1972) 4709.
[44] H. Li, Y. Guo, J. Robertson, Calculation of TiO2 surface and subsurface oxygen vacancy by the screened exchange functional, J. Phys. Chem. C 119 (2015) 18160–18166.
[45] C.T. Sah, Electronic processes and excess currents in gold-doped narrow silicon junctions, Phys. Rev. 123 (1961) 1594.
[46] J.-H. Kim, W.-J. Lee, J.-D. Kim, S.-G. Yoon, Influence of laser treatment on the electrical properties of plasma-enhanced-atomic-layer-deposited TiO2 thin films, Met. Mater. Int. 11 (2005) 285–289.
[47] H.Y. Jeong, J.Y. Lee, S. Choi, Interface-engineered amorphous TiO2-based resistive memory devices, Adv. Funct. Mater. 20 (2010) 3912–3917.
[48] S. Won, S. Go, W. Lee, K. Jeong, H. Jung, C. Lee, E. Lee, J. Lee, Effects of defects generated in ALD TiO2 films on electrical properties and interfacial reaction in TiO2/SiO2/Si system upon annealing in vacuum, Met. Mater. Int. 14 (2008) 759–765.
[49] M. Mikami, S. Nakamura, O. Kitao, H. Arakawa, X. Gonze, First-principles study of titanium dioxide: rutile and anatase, Jpn. J. Appl. Phys. 39 (2000) L847.
[50] N. Alimardani, S.W. King, B.L. French, C. Tan, B.P. Lampert, J.F. Conley Jr., Investigation of the impact of insulator material on the performance of

dissimilar electrode metal-insulator-metal diodes, J. Appl. Phys. 116 (2014) 024508.
[51] A.M. Eppler, I.M. Ballard, J. Nelson, Charge transport in porous nanocrystalline titanium dioxide, Phys. E Low Dimens. Syst. Nanostruct. 14 (2002) 197–202.
[52] A.F. Halverson, K. Zhu, P.T. Erslev, J.Y. Kim, N.R. Neale, A.J. Frank, Perturbation of the electron transport mechanism by proton intercalation in nanoporous TiO2 films, Nano Lett. 12 (2012) 2112–2116.
[53] R.S. Williams, How we found the missing memristor, IEEE Spectr. 45 (2008).
[54] D.B. Strukov, G.S. Snider, D.R. Stewart, R.S. Williams, The missing memristor found, Nature 453 (2008) 80–83.
[55] D.R. Stewart, D.A.A. Ohlberg, P.A. Beck, Y. Chen, R.S. Williams, J.O. Jeppesen, K.A. Nielsen, J.F. Stoddart, Molecule-independent electrical switching in Pt/organic monolayer/Ti devices, Nano Lett. 4 (2004) 133–136.
[56] P. Heljo, K. Wolff, K. Lahtonen, M. Valden, P.R. Berger, H. Majumdar, D. Lupo, Anodic oxidation of ultra-thin Ti layers on ITO substrates and their application in organic electronic memory elements, Electrochim. Acta 137 (2014) 91–98.